Particle & Particle Systems Characterization
www.particle-journal.com

Au–Pd Alloy Octapods with High Electrocatalytic Activity for the Oxidation of Formic Acid

Liang-Bing Wang, You-Cheng Wang, Hong-Yan Guo, Jian-Liu Huang, Yun-Long Zhao, Qi-Yu Liu, Xiaojun Wu, and Jie Zeng**

The synergy created by different metals, which can be essentially accredited to lattice effects and heteroatom bonding, is usually difficult to know a prior about.[1–6] According to the remarkable contributions by many research groups, Au–Pd bimetallic nanocrystals displayed enhanced catalytic performances than their monometallic counterparts in diverse situations.[7–10] From a simplified perspective, these synergistic effects can be accredited to intrinsically high catalytic activity of both Au and Pd towards various reactions and the notably excellent catalytic stability of Au against poisoning.[11–14] In an attempt to optimize the bimetallic synergy between Au and Pd, however, it is inevitable to pay regard to other determining parameters including structure, size, and shape, among which shape is mostly studied. Controlling the shape is one of the key strategies to manipulating the exposed facets and spatial distribution of atoms and therefore critical to physicochemical properties.[15–39] For example, the multipods shape attracts special research interest due to comparatively large specific surface area and a rough surface on branches. Since the rough surface is often correlated with high density of atomic steps, kinks, and other defects, or equivalently, high-index feature, multipods are generally expected to show higher catalytic or electrocatalytic activity than most of the other shapes with a similar size.[40–43] Nevertheless, primarily because the multipod shape is thermodynamically unfavorable in solution-phase synthesis and the growth process of bimetallic nanocrystals involves complicated coupling of kinetic factors, controlled preparation of Au-Pd nanocrystals in a multipod shape has been rarely reported in literature.

Here, we report a facile route to the synthesis of Au–Pd alloy octapods with the exposure of high-index {722} facets employing a seed-meditated growth protocol. Through simply adjusting the amount of addition of seeds, we obtained Au–Pd alloy octapods with uniform spanning size in the range of 25–120 nm. The formation mechanism of octapods was explored by manipulating the concentration of H^+ and reaction temperature. In general, unduly high or low concentrations of H^+ and elevated reaction temperature were found to be injurious to the formation of Au–Pd octapods, which could be ascribed to kinetic or thermodynamic reasons. The as-prepared Au–Pd alloy octapods manifested superior catalytic activity in electro-oxidation of formic acid (HCOOH). It was further revealed by first-principles calculations that the substitution of Au by Pd on Au {722} facet gives rise to higher adsorption energy of molecular HCOOH and $HCOO^-$, and thus higher activity for the reaction.

In the first step, Au seeds about 2–3 nm in size were prepared by reducing $HAuCl_4$ with $NaBH_4$ in an aqueous solution in the presence of cetyltrimethylammonium bromide (CTAB) as a capping agent at room temperature (ca. 25 °C). The solution was diluted 500 fold with ultrapure water prior to be used as seeds. The growth solution was then prepared by consecutively adding 0.1 mL of 10×10^{-3} M $HAuCl_4$, 0.1 mL of 10×10^{-3} M Na_2PdCl_4, 100 μL of 1 M HCl, and then 200 μL of 100×10^{-3} M L-ascorbic acid (AA) to a 10 mL aqueous solution of 100×10^{-3} M cetyltrimethylammonium chloride (CTAC). 100 μL of Au seeds was then introduced to initiate the reaction, after which the solution was swirled immediately. The reaction was allowed to proceed undisturbed at 25 °C for 30 min. **Figure 1**A shows a representative scanning electron microscopy (SEM) image of the as-synthesized nanocrysals, indicating these uniform eight-armed star-like nanocrystals with spanning size (see the definition in Figure S1, Supporting Information) of 55 ± 4 nm are in high purity. Figure 1B and C show transmission electron microscopy (TEM) and scanning transmission electron microscopy (STEM) images of the products, respectively, which ensures better visualization of their 3D structure. The brighter four arms and darker center part reveal the concave feature of the structure. The morphological characteristics of the nanocrystals were fully examined by TEM tilted along three different zone axis (i.e., [100], [111], and [110]), aided by selected-area electron diffraction (SAED) to guarantee the accurate orientation. Figure 1D–L presents TEM images, the corresponding SAED patterns, and oriented geometric models of the Au–Pd alloy octapods viewed along the three directions. As shown in Figure 1D and G, the apex angles of the trigonal-pyramidal arms oriented along [100] and [111] were measured to be 47° and 53°, respectively. When projected along [110], the alloy octapods appeared in the shape of elongated six-armed

L.-B. Wang,[†] Y.-C. Wang,[†] H.-Y. Guo, J.-L. Huang, Y.-L. Zhao, Q.-Y. Liu, Prof. X. Wu, Prof. J. Zeng
Hefei National Laboratory for Physical Sciences at the Microscale
Collaborative Innovation Center of Suzhou Nano Science and Technology
Center of Advanced Nanocatalysis (CAN-USTC)
CAS Key Lab of Materials for Energy Conversion
Synergetic Innovation Center of Quantum Information and Quantum Physics
School of Chemistry and Materials Science
University of Science and Technology of China
Hefei, Anhui 230026, P. R. China
E-mail: xjwu@ustc.edu.cn; zengj@ustc.edu.cn
[+]These authors contributed equally.

DOI: 10.1002/ppsc.201400130

Particle
& Particle Systems Characterization
www.particle-journal.com

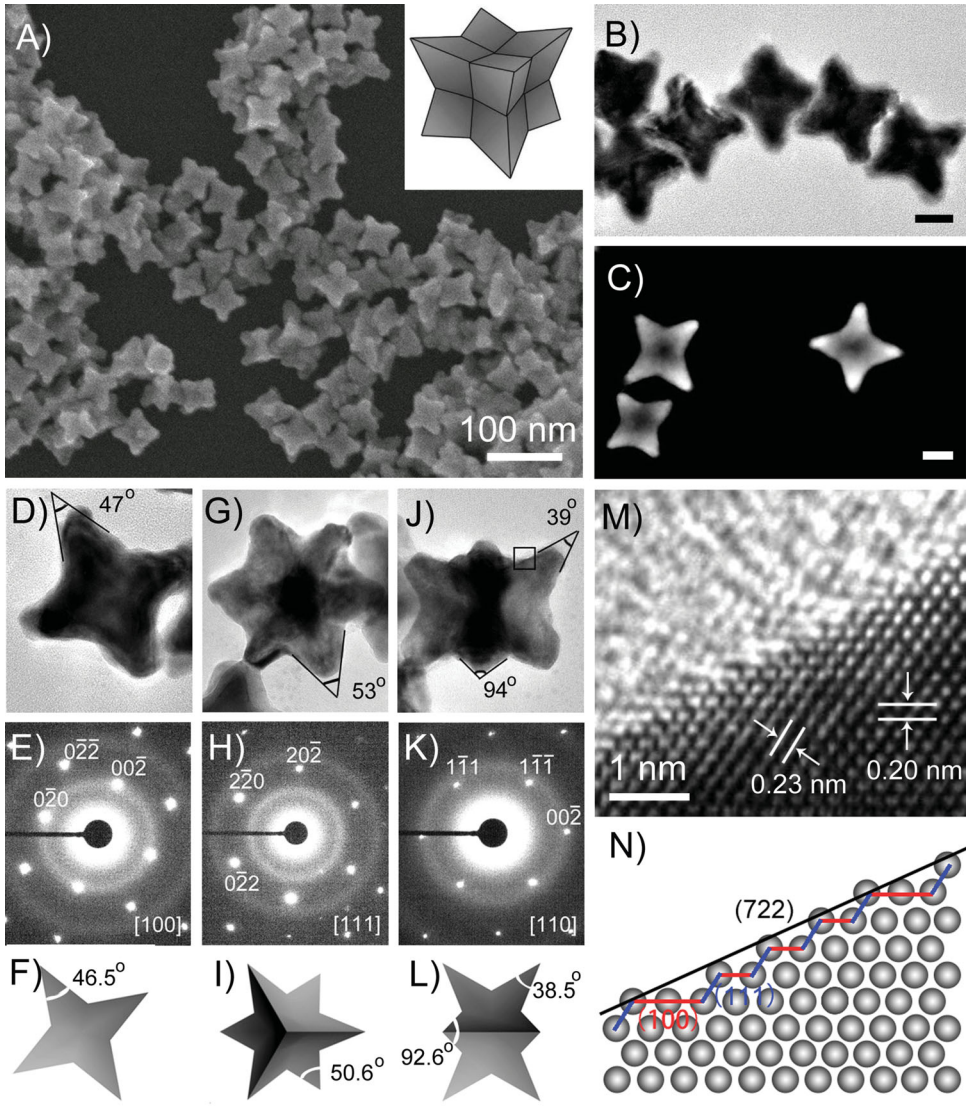

Figure 1. Synthesis of Au–Pd octapods through seed-mediated overgrowth. A) SEM, B) TEM, and C) HAADF-STEM images of Au-Pd octapods. D,G,J) TEM images, E,H,K) SAED patterns, and F,I,L) geometric models of individual octapods oriented along the D-F) [100], G-I) [111], and J–L) [110] directions. M) HRTEM image and N) atomic model of the region indicated by the box in (J). The inset image in panel A is a model of octapod. The scale bars in panel B and C correspond to 20 nm.

stars, with four longer arms on two sides and two shorter ones in the middle, the apex angles of which were surveyed to be 39° and 94°, respectively. Geometric models (Figure 1F, I, and L) was proposed to accord with the contour of alloy octapods projected along the three different directions in Figure 1 D, G, and J, respectively. The Miller indices of symmetrical exposed facets can be determined by analyzing the apex angle of the trigonal-pyramidal arms to be {722}. In addition, they can also be determined from straight observation of atomic steps. Figure 1M shows high-resolution transmission electronic microscopy (HRTEM) image of the atomic arrangement of an octapod. Because of the close proximity of the radius of Au and Pd atoms, the relationship between lattice spacing and Miller indices can be found out with ease. When the kite-shaped face of an arm of octapods were directed perpendicular to the electron beam, two sets of fringes with lattice spacing of 2.3 Å and 2.0 Å were observed, relating to the {111} and {200} planes, respectively. Figure 1N represents atomic model of Figure 1M. The atomic arrangement periodically consisted of a series of {111} terraces and {200} terraces. By counting the atomic widths, the overall profile were indexed as the {722} plane, which matches with the projection angles.

The composition of the as-synthesized nanocrystals was examined by X-ray diffraction (XRD) and elemental mapping analysis using scanning transmission electron microscopy–energy-dispersive X-ray spectrometry (STEM–EDX). As shown in **Figure 2**A and Figure S2 (Supporting Information), the XRD peaks of the as-synthesized Au–Pd alloy octapods, pure Au and Pd nanocrystals can be indexed as face-centered cubic (fcc) structure. Notably every diffraction peak of the octapods lies amongst the peak positions of pure fcc Au (JCPDS no. 04-0784) and Pd (JCPDS no. 05-0681), proposing the successful

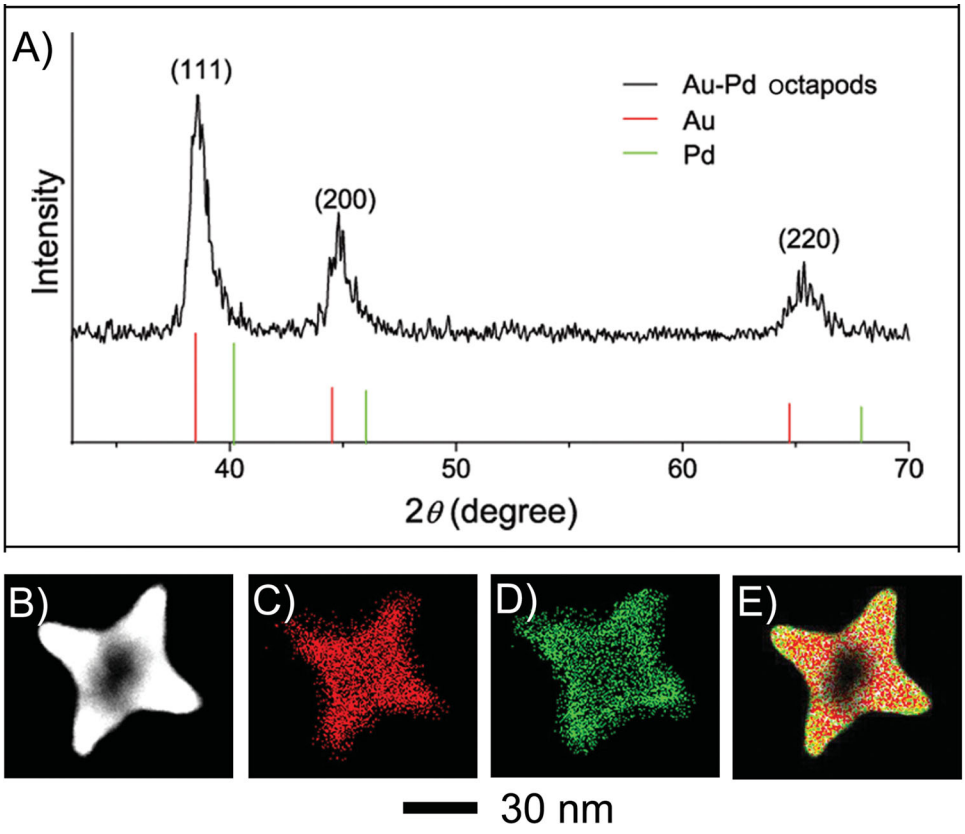

Figure 2. Compositional analysis of the as-prepared Au-Pd octapods. A) XRD pattern, B) STEM image, C,D) STEM–EDX elemental mapping of C) Au, and D) Pd, and E) merged image of an individual Au-Pd alloy octapod. The Au atoms are shown in red and Pd atoms are shown in green.

preparation of Au–Pd alloy octapods. Using the least-squares method, the lattice parameter of the octapods was calculated to be 4.06 Å. According to Vegard's law, which claims the linear relation between the lattice parameter of an alloy and its composition, the Pd content in Au–Pd octapods was estimated to be 15%.[44] The Pd content was further determined by inductive coupled plasma–atomic emission spectroscopy (ICP-AES) to be 16.2%. Figure 2B is a magnified STEM image of a typical Au–Pd alloy octapod, on which elemental mapping analysis was induced. The results (Figure 2C–E) clearly demonstrate the ubiquitous distribution of both Au (Figure 2C) and Pd (Figure 2D). The merged image (Figure 2E) associated with the cross-sectional compositional line-scanning profile (Figure S3, Supporting Information) further confirmed the almost completely overlapping of distribution range of the two metal components. That the two metals distribute in accordance with each other excludes core–shell or hybrid structures. The above analysis confirms the successful preparation of Au–Pd alloy octapods.

Au seeds of other different amounts were also employed to grow Au–Pd alloy octapods to achieve valid size control. Figure S4 (Supporting Information) displays Au–Pd alloy octapods synthesized via the method mentioned beforehand, differing only in the amount of seed included in the nucleation stage of the reaction. From Figure S4A to S4D (Supporting Information), 1000, 250, 70, and 35 µL of diluted seeds were supplied, respectively. Correspondingly, Au–Pd alloy octapods with the average spanning size of 25 ± 5, 45 ± 10, 70 ± 12, and 120 ± 20 nm were successfully prepared. The results suggest that fewer seeds lead to larger structures, which could be accredited to fewer nucleation sites and more plentiful precursors. Although these particles vary in spanning size, they remain the concave feature and high-index facets. Moreover, a high yield above 85% was observed for the synthesized octapods in all sizes. This suggests that the size of the Au–Pd alloy octapods could be controlled over a broad range by briefly using different amount of seeds.

In elucidating the mechanism involved in the preparation of Au–Pd alloy octapods, we devised a set of experiments using the standard procedure except for a modulation of the H^+ concentration or reaction temperature. As illustrated in Figure S5 (Supporting Information), the products were highly sensitive to the amount of HCl, which is correlated to pH and thus the reducing capacity of AA. Generally, when less HCl is put into the reaction system, the pH will become higher, and then the reduction capacity of AA will be stronger. Figure S5A and B (Supporting Information) show nanocrystals obtained with 0 and 20 µL of HCl, respectively, both amounts of which were much less than standard (100 µL). The products turned to be coarse particles about 50 nm in size with complex prods. These prods were 5–10 nm in length around the particle. However, for samples with more HCl relative to those used in the standard synthesis, smooth structures with blunt ends on the arms evolved (Figure S5D, Supporting Information). As shown in

Figure S6 (Supporting Information), reaction temperature was also discovered to have essential influence on the shape of the product. When synthesis was performed at 80 °C, the products appeared as flat polyhedrons (Figure S6, Supporting Information) including octahedrons and truncated bipyramids mainly enclosed by {111} facets on the surface.

These results are kinetically or thermodynamically comprehensible. When AA was introduced into the aqueous solution, it immediately reduced the salt precursors, namely Au^{3+} and Pd^{2+}, to Au^{+} and Pd atoms. Au^{+} ions subsequently undergo disproportionation reaction catalyzed by the surface of metallic gold (seeds or growing nanocrystals). On condition that a smaller amount of HCl or no HCl is added, the concentration of H^{+} of the solution is expected to be lower, and so reduction capacity of AA will be higher. Due to fast reduction, more nucleation sites on a seed can be generated, ultimately forming coarse structured nanocrystals with more prods. Instead, larger amount of HCl depresses reduction rate, preventing formation of multiple nucleation sites as a consequence. Therefore, growth of a seed tended to preferentially occurs in specific regions with higher activity, evolving into less irregular structures with a smooth surface. The phenomenon that polyhedrons survived when reaction temperature was adjusted to be 80 °C can be attributed to the fact that they are enclosed by {111} facets with lower surface energy and thus thermodynamically favored.

The Au–Pd alloy octapods 55 nm in average spanning size with {722} high-index facets were evaluated as a catalyst for electro-oxidation of formic acid. As a benchmark, the electrocatalytic ability of Au–Pd polyhedrons (Figure S6, Supporting Information) obtained at 80 °C, commercial catalyst Pd/C (Figure S7, Supporting Information), and Pd black were tested under the same circumstances. To normalize current densities and then enable direct comparison of catalytic activities, the electrochemically active surface areas (ECSAs) of the samples were firstly surveyed through hydrogen adsorption (Figure S8, Supporting Information). **Figure 3**A and Figure S9 (Supporting Information) shows normalized cyclic voltammetry (CV) curves measured on glassy carbon electrodes loaded with Au–Pd alloy octapods, Au–Pd polyhedrons, Pd/C, or Pd black at room temperature in a solution containing 0.50 M H_2SO_4 and 0.25 M HCOOH. The electro-catalytic activity of Au–Pd alloy octapods was far superior to those of the other catalysts, with peak current density 2.6 times, 5.1 times, and 5.9 times higher than Au–Pd polyhedrons, Pd/C, and Pd black, respectively. The {722} high-index facets of octapods should account for the enhanced catalytic activity towards formic acid oxidation. Furthermore, the Au–Pd octapods were found to maintain better stability (Figure 3B) in catalytic performance than Au–Pd polyhedrons and Pd/C. ICP dates indicated that the compositions of these catalysts were not changed, while SEM and TEM images (Figure S10, Supporting Information) showed that the catalysts maintained their structure after durability test. According to the works reported before,[9] the alloying of Au could enhance the stability and durability of Pt- or Pd-based catalysts for electrochemistry catalysis. Therefore, we consider that Au–Pd alloy improves the formic acid tolerance.

To gain some insight into the enhanced catalytic properties of Au–Pd alloy octapods with the exposure of {722} facets, we investigated the adsorption of molecular HCOOH on Au {722} surface with Pd_n (n = 0, 1, 2, or 4) atoms substituting Au atoms along the direction of one Au atomic chain per supercell.[45,46] Since desorption of H^{+} from HCOOH should occur, we also examined the adsorption of molecular $HCOO^{-}$. Based on the density functional calculations, the most favorable configurations for molecular HCOOH and $HCOO^{-}$ adsorbed on Pd-substituted Au {722} surfaces are plotted in **Figure 4**. When HCOOH attaches to pure Au {722} surface (n = 0), it prefers a top-hollow orientation (Figure 4A, left panel), which means that one oxygen atom locates on top of an Au atom while the OH group points to a hollow site. As shown in the left panels of Figure 4B–D, the configurations of HCOOH adsorption on Au {722} surface with Pd_1, Pd_2, and Pd_4 substitution per supercell appear to be distorted compared with that of pure Au {722} surface. However, the top-hollow orientation is largely preserved as a result of strong ionic bonding between O and metal atoms. Interestingly, HCOOH selectively bonds with Pd atoms instead of Au atoms because of higher adsorption energy. In the case of $HCOO^{-}$ adsorbed on pure and Pd-substituted Au {722} surface, however, $HCOO^{-}$ tends to adsorb along the direction of one atomic chain (Figure 4A–D, right panels). In supercells with Pd-substitution, $HCOO^{-}$ also preferentially bonds with Pd atoms. The calculated adsorption energies (in eV, please

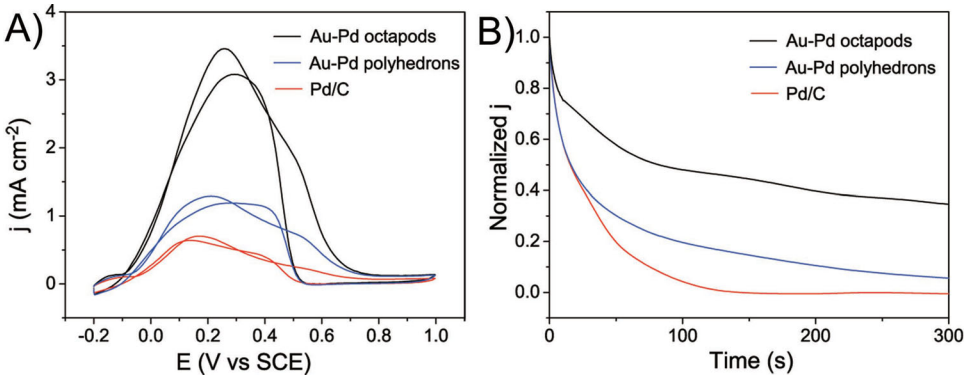

Figure 3. A) CV curves measured on Au–Pd alloy octapods, polyhedrons, and Pd/C in 0.50 M H_2SO_4 + 0.25 M HCOOH solution, respectively. Scanning rate is 50 mV s^{-1}. B) current–time curves of formic acid oxidation measured on the three kinds of catalysts in 0.50 M H_2SO_4 + 0.25 M HCOOH solution at 0.20 V. All current values were normalized with respect to the ECSA. The current densities in electrocatalytic stability measurements have been normalized with respect to initial values of the three samples.

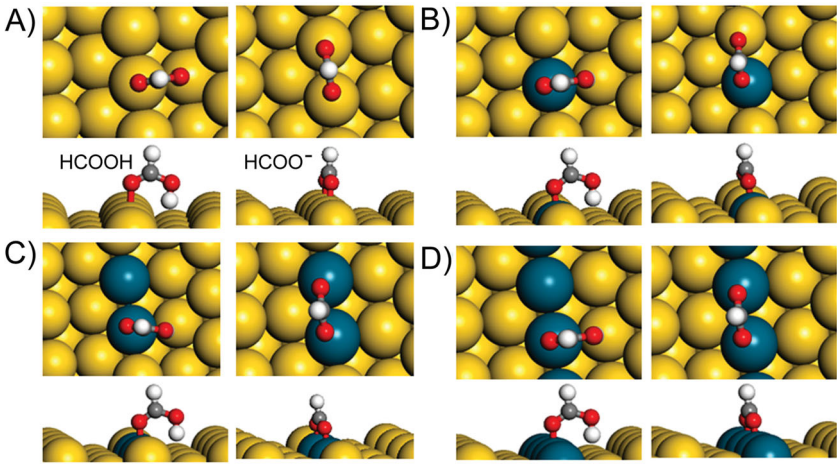

Figure 4. The most stable configurations for HCOOH and $HCOO^-$ adsorbed on A) Au {722} surface without Pd and with B) one, C) two, and D) four Pd atoms per supercell, respectively. For each configuration, the upper and the lower drawings display the top and side view, respectively, and the left and the right drawings display HCOOH and $HCOO^-$ adsorption configurations, respectively.

see the definition in Supporting Information) of HCOOH and $HCOO^-$, and Pd-O or Au-O distance (Å) on pure/Pd-substituted Au {722} surfaces are summarized in **Table 1** and Table S1 (Supporting Information), respectively. It can be identified that the adsorption of HCOOH on pure Au {722} surfaces is weak with the energy value of –0.34 eV. The negative values indicate that the adsorption is exothermic. The substitution of Pd on Au {722} surface enhances the adsorption energy to a moderate value ranging from –0.56 to –0.60 increasing with the atomic number of Pd_n (n = 1, 2, and 4). The adsorption of HCOOH with moderate adsorption energy is a crucial factor to the enhancement of electrocatalytic activity. Meanwhile, the corresponding adsorption energy of $HCOO^-$ shows an evident trend of similar increase with the atomic number of Pd_n (n = 0, 1, 2, and 4) chain. With the assumption that desorbed H^+ is captured by OH^- in the electrochemical reaction, it was discovered that the released reaction energy increases significantly when n is changed from 2 to 4, which can enhance the electrocatalytic activity as a thermodynamic factor.

In summary, we have achieved a facile synthesis of Au–Pd alloy octapods encased by {722} facets via a seed-meditated growth process. Through regulating the amount of seeds in growth, we were able to effectively control the spanning size of octapods. Formation of the octapods is discovered to be sensitive to the concentration of H^+ and reaction temperature in the synthesis, demonstrating kinetic and thermodynamic control of the growth, respectively. Compared with Au–Pd polyhedrons enclosed mainly by low-index {111} facets and Pd/C, Au–Pd alloy octapods exhibited substantially enhanced catalytic activity towards the electro-oxidation of formic acid. Moreover, according to first-principles computations, the substitution of Au by Pd atoms on Au {722} facets can enhance adsorption of reactant molecules (HCOOH and $HCOO^-$), and the enhanced electrocatalytic activity can be partly understood with this thermodynamic factor. Our approach based on seed-meditated overgrowth can promisingly be extended to other metallic systems to generate multipod shape and probably high-index feature, and thus high activities towards various important reactions.

Table 1. Calculated adsorption energies (*AEs*, in eV) of HCOOH molecular and $HCOO^-$ adsorbed on Au {722} surface without Pd and with one, two and four Pd atoms, respectively.

	Pd_0	Pd_1	Pd_2	Pd_4
HCOOH	–0.34	–0.56	–0.58	–0.60
$HCOO^-$	–2.13	–2.38	–2.64	–2.73

Supporting Information

Supporting Information is available from the Wiley Online Library or from the author.

Acknowledgements

This work was supported by MOST of China (2014CB932700, 2011CB921403, and 2012CB922001), NSFC under grant Nos. 21203173, 51371164, 21121003, and J1030412, Strategic Priority Research Program B of the CAS under grant No. XDB01020000, and Fundamental Research Funds for the Central Universities (WK2340000050, WK2060190025, and WK2060140014).

Received: June 17, 2014
Revised: August 14, 2014
Published online: September 10, 2014

[1] P. D. Cozzoli, T. Pellegrino, L. Manna, *Chem. Soc. Rev.* **2006**, *35*, 1195.
[2] R. Ferrando, J. Jellinek, R. L. Johnston, *Chem. Rev.* **2008**, *108*, 845.
[3] L. Carbone, P. D. Cozzoli, *Nano Today* **2010**, *5*, 449.
[4] D.Wang, Y. Li, *Adv. Mater.* **2011**, *23*, 1044.
[5] R. Costi, A. E. Saunders, U. Banin, *Angew. Chem. Int. Ed.* **2010**, *49*, 4878.
[6] J. Zeng, C. Zhu, J. Tao, M. Jin, H. Zhang, Z. Y. Li, Y. Zhu, Y. Xia, *Angew. Chem. Int. Ed.* **2012**, *51*, 2354.
[7] L. Kesavan, R. Tiruvalam, M. H. Ab Rahim, M. I. bin Saiman, D. I. Enache, R. L. Jenkins, N. Dimitratos, J. A. Lopez-Sanchez, S. H. Taylor, D. W. Knight, C. J. Kiely, G. J. Hutchings, *Science* **2011**, *331*, 195.
[8] Y. W. Lee, M. Kim, S. W. Kang, S. W. Han, *Angew. Chem. Int. Ed.* **2011**, *123*, 3528.
[9] L. Zhang, J. Zhang, Q. Kuang, S. Xie, Z. Jiang, Z. Xie, L. Zheng, *J. Am. Chem. Soc.* **2011**, *133*, 17114.
[10] L. F. Zhang, S. L. Zhong, A. W. Xu, *Angew. Chem. Int. Ed.* **2013**, *52*, 645.
[11] A. A. Herzing, C. J. Kiely, A. F. Carley, P. Landon, G. J. Hutchings, *Science* **2008**, *321*, 1331.
[12] A. Wittstock, V. Zielasek, J. Biener, C. M. Friend, M. Baumer, *Science* **2010**, *327*, 319.
[13] Y. Wan, H. Wang, Q. Zhao, M. Klingstedt, O. Terasaki, D. Zhao, *J. Am. Chem. Soc.* **2009**, *131*, 4541.

[14] J. Zhang, K. Sasaki, E. Sutter, R. R. Adzic, *Science* **2007**, *315*, 220.
[15] R. L. Chantry, I. Atanasov, W. Siriwatcharapiboon, B. P. Khanal, E. R. Zubarev, S. L. Horswell, R. L. Johnston, Z. Y. Li, *Nanoscale* **2013**, *5*, 7452.
[16] J. Zhang, M. R. Langille, M. L. Personick, K. Zhang, S. Li, C. A. Mirkin, *J. Am. Chem. Soc.* **2010**, *132*, 14012.
[17] L. Vigderman, E. R. Zubarev, *Langmuir* **2012**, *28*, 9034.
[18] C. J. DeSantis, S. E. Skrabalak, *Langmuir* **2012**, *28*, 9055.
[19] X. Huang, Y. Li, Y. Li, H. Zhou, X. Duan, Y. Huang, *Nano Lett.* **2012**, *12*, 4265.
[20] G. H. Wang, J. Hilgert, F. H. Richter, F. Wang, H. J. Bongard, B. Spliethoff, C. Weidenthaler, F. Schuth, *Nat. Mater.* **2014**, *13*, 294.
[21] B. T. Sneed, C. N. Brodsky, C. H. Kuo, L. Lamontagne, K. Y. Jiang, Y. Wang, F. Tao, W. Huang, C. K. Tsung, *J. Am. Chem. Soc.* **2013**, *135*, 14691.
[22] H. You, S. Yang, B. Ding, H. Yang, *Chem. Soc. Rev.* **2013**, *42*, 2880.
[23] Y. Yin, D. Talapin, *Chem. Soc. Rev.* **2013**, *42*, 2484.
[24] Z. Quan, Y. Wang, J. Fang, *Acc. Chem. Res.* **2011**, *46*, 191.
[25] J. Zhang, M. R. Langille, M. L. Personick, K. Zhang, S. Li, C. A. Mirkin, *J. Am. Chem. Soc.* **2010**, *132*, 14012.
[26] H. Zhang, W. Li, M. Jin, J. Zeng, T. Yu, D. Yang, Y. Xia, *Nano Lett.* **2011**, *11*, 898.
[27] X. Huang, Z. Zhao, J. Fan, Y. Tan, N. Zheng, *J. Am. Chem. Soc.* **2011**, *133*, 4718.
[28] X. Xia, J. Zeng, B. McDearmon, Y. Zheng, Q. Li, Y. Xia, *Angew. Chem. Int. Ed.* **2011**, *50*, 12542.
[29] X. Huang, S. Tang, H. Zhang, Z. Zhou, N. Zheng, *J. Am. Chem. Soc.* **2009**, *131*, 13916.
[30] F. Wang, C. H. Li, L. D. Sun, H. S. Wu, T. A. Ming, J. F. Wang, J. C. Yu, C. H. Yan, *J. Am. Chem. Soc.* **2011**, *133*, 1106.
[31] Z. Quan, Z. Luo, Y. Wang, H. Xu, C. Wang, Z. Wang, J. Fang, *Nano Lett.* **2013**, *13*, 3729.
[32] F. Lu, Y. Zhang, L. Zhang, Y. Zhang, J. X. Wang, R. R. Adzic, E. A. Stach, O. J. Gang, *J. Am. Chem. Soc.* **2011**, *133*, 18074.
[33] Y. Wu, D. Wang, Y. Li, *Chem. Soc. Rev.* **2014**, *43*, 2112.
[34] C. L. Lu, K. S. Prasad, H. L. Wu, J. A. A. Ho, M. H. Huang, *J. Am. Chem. Soc.* **2010**, *132*, 14546.
[35] C. J. DeSantis, A. A. Peverly, D. G. Peters, S. E. Skrabalak, *Nano Lett.* **2011**, *11*, 2164.
[36] J. Zhang, Y. Tang, L. Weng, M. Ouyang, *Nano Lett.* **2009**, *9*, 4061.
[37] B. Senyuk, J. S. Evans, P. J. Ackerman, T. Lee, P. Manna, L. Vigderman, E. R. Zubarev, J. van de Lagemaat, I. I. Smalyukh, *Nano Lett.* **2012**, *12*, 955.
[38] B. T. Sneed, C. H. Kuo, C. N. Brodsky, C. K. Tsung, *J. Am. Chem. Soc.* **2012**, *134*, 18417.
[39] H. Zhu, S. Zhang, S. Guo, D. Su, S. Sun, *J. Am. Chem. Soc.* **2013**, *135*, 7130.
[40] Y. Jia, Y. Jiang, J. Zhang, L. Zhang, Q. Chen, Z. Xie, L. Zheng, *J. Am. Chem. Soc.* **2014**, *136*, 3748.
[41] X. Huang, Y. Li, Y. Chen, E. Zhou, Y. Xu, H. Zhou, X. Duan, Y. Huang, *Angew. Chem. Int. Ed.* **2013**, *52*, 2520.
[42] B. Lim, M. Jiang, P. H. C. Camargo, E. Cho, J. Tao, X. Lu, Y. Zhu, Y. Xia, *Science* **2009**, *324*, 1302.
[43] Z. Peng, H. Yang, *Nano Today* **2009**, *4*, 143.
[44] A. R. Denton, N. W. Ashcroft, *Phys. Rev. A* **1991**, *43*, 3161.
[45] B. Delley, *J. Chem. Phys.* **1990**, *92*, 508.
[46] B. Delley, *J. Chem. Phys.* **2003**, *113*, 7756.